Simulation of Nonlinear Optical Effects in Photonic Crystals Using the Finite-Difference Time-Domain Method

A Thesis
Presented to
The Academic Faculty

By

Charles M. Reinke

In Partial Fulfillment
Of the Requirements for the Degree
Master of Science in Electrical Engineering

Georgia Institute of Technology
May 2007

Simulation of Nonlinear Optical Effects in Photonic Crystals Using the Finite-Difference Time-Domain Method

Approved by:

Dr. Ali Adibi
School of Electrical and Computer Engineering
Georgia Institute of Technology

Dr. John Buck
School of Electrical and Computer Engineering
Georgia Institute of Technology

Dr. Thomas Gaylord
School of Electrical and Computer Engineering
Georgia Institute of Technology

Date Approved: March 27th, 2007

Acknowledgements

Of all the things that seemed to fall into place when I was starting my graduate student career, one of the most significant was being selected a new professor at Georgia Tech to join his research group. Working with Dr. Ali Adibi has proved to be a great opportunity, as he strived to make my time at Georgia Tech as profitable as possible. I am overwhelmed with appreciation for his time, knowledge, and commitment to me as my advisor.

I would also like to thank Dr. Sina Khorasani for his invaluable assistance during the early stages of this research project. He had the vision to see what it could become, and taught me much about nonlinear optics and numerical electromagnetics along the way. I only wish that our time working together at Georgia Tech could have been longer. Also, I appreciate Dr. Reginald Lee and Dr. Yong Xu for the use of their finite-difference time-domain code, and several helpful discussions regarding it and the technique in general.

I am greatly indebted to my parents for all of the love, support, and wisdom they have offered me during me throughout my life and grad school years in particular. Without them I would certainly not be where I am today, and without their prayers would likely not have endured through my graduate studies.

Finally, I would like to thank God Almighty, Who made me who I am, empowers me in all of my successes by His Son Yeshua, and guides my through my life journey through His Spirit.

Table of Contents

List of Figures

Summary

The phenomenon of polarization interaction in certain nonlinear materials is presented, and the design of an all-optical logic device based on this concept is described. An efficient two-dimensional finite-difference time-domain code for studying third-order nonlinear optical phenomena is discussed, in which both the slowly varying and the rapidly varying components of the electromagnetic fields are considered. The algorithm solves the vector form Maxwell's equations for all field components and uses the nonlinear constitutive relation in matrix form as the equations required to describe the nonlinear system. The stability of the code is discussed and its accuracy demonstrated through the simulation of the self-phase modulation effect observed in Kerr media. Finally, the code is used to simulate polarization mixing in photonic crystal-based line defect and coupled resonator optical waveguides.

Chapter 1
Introduction

Nonlinear optics has a wide range of applications in many areas such as communications and optical computing [1]. Of particular interest, we can use nonlinear optical materials to achieve all-optical control of electromagnetic waves, which can lead to all-optical signal processing. Nonlinear optics also has a number of inherent benefits, such as the ability to compensate for linear dispersion and diffraction effects, as evidenced by temporal and spatial solitons [2]. Utilizing the nonlinear properties of various materials, optical switches and modulators have also been realized and found wide applications in modern telecommunication industries [3,4].

The implementation of all-optical logic based on the nonlinear interactions is a much sought-after goal. One possible approach to achieve all-optical logic is to take advantage of the property of $\chi^{(3)}$ nonlinear materials where transverse-electric (TE) and transverse-magnetic (TM) polarizations can exchange energy when they are present simultaneously. This nonlinear coupling between TE and TM polarizations is unidirectional in planar semiconductor waveguides, i.e. the electromagnetic energy tends to transfer from TM to TE modes only. All-optical logic gates based on four-wave mixing have been discussed by several research groups [5-7], but appreciable results have not been shown, and the discussions have mostly been limited to theoretical modeling and system implementation, rather than actual device design. The major drawback of these systems has been that the logic operation is necessarily done using lights sources at multiple frequencies. In practice, however, the requirement for single frequency amplification or single frequency logic demands a different approach.

Recently, photonic crystal (PC) structures have also been extensively investigated in literature [8-13]. One of the most useful features of PC structures is that for a large enough index contrast, a PC can exhibit a photonic bandgap, i.e. a range of frequencies within which a propagating electromagnetic wave does not exist [14-18]. More practically, PC structures are also interesting because they allow for precise control of electromagnetic wave propagation, as exemplified in the studies of sharp bends [19], nano-scale optical cavities [20], and add-drop filters [21].

Thus, the investigation of optical information processing has become a popular trend in photonic crystal (PC) research. As electromagnetic counterparts of electronic circuits, PCs are expected to handle the most essential operations in the realization of optical computing, via nonlinear optical processes. Since PC structures can support electromagnetic modes with unique modal profiles and drastically differing dispersion properties, the introduction of nonlinear materials into PC structures has led to many interesting nonlinear optical phenomena [22-32]. Power transfer between TE and TM polarizations has been demonstrated in simulations of both a conventional dielectric slab waveguide and a W1 PC waveguide, where the waveguide is formed by removed a single row of air holes in the PC lattice. It has also been shown that improvement of the power transfer should occur in PC waveguides where the lower group velocity allows for slow-light enhancement [33], for example resonator-based devices.

As a result, it is of critical importance to use a numerical algorithm that can easily and accurately simulate nonlinear optical process in complex dielectric structures such as photonic crystals. A very common technique for the analysis of nonlinear optical wave propagation is the nonlinear Schrödinger equation, due to its ability to provide analytical

results. Unfortunately, it is generally difficult to use the nonlinear Schrödinger equation to describe wave propagation in PCs, since PC structures typically have very large index contrast and exhibit significant modal dispersion (especially near the band edge), which invalidates some basic approximations in the derivation of the nonlinear Schrödinger equation [34]. The finite-difference time-domain (FDTD) method of analysis [35], however, is applicable for a wide range of complex dielectric structures, constrained only by the size of the computational space required for the simulation. Several FDTD-based algorithms have been developed to address nonlinear phenomena, including FDTD formulations by Sullivan [36] for nonlinear dispersive optical structures that utilizes Z transforms and Tran [37,38] for simple Kerr media.

Therefore, a nonlinear two-dimensional finite-difference-time-domain (2-D FDTD) code based on a modification of Yee's original FDTD algorithm has been developed that is suitable for simulating the effects of third-order nonlinearity in arbitrary PC structures. This code has been optimized by focusing only on $\chi^{(3)}$ materials of interest and by assuming that the nonlinear effects are instantaneous. Thus, it offers better computational efficiency over other nonlinear FDTD methods, at the expense of a small loss of generality in application. The stability of the code is demonstrated and several simulation results are offered. This discussion begins with an overview of the basic FDTD algorithm and a description of the nonlinear extension to the original linear method. Here, the techniques used and the limitations of the method are presented. A straightforward analysis of the stability of our code under the linear conditions is given next, followed by qualitative and quantitative verification of the generated results.

Chapter 2
Polarization Coupling in $\chi^{(3)}$ Materials

To illustrate the basic idea, consider the nonlinear constitutive relation for simple $\chi^{(2)}$ nonlinear materials:

$$\begin{bmatrix} D_x \\ D_y \\ D_z \end{bmatrix} = \begin{bmatrix} \varepsilon_x & \frac{1}{2}\chi^{(2)}E_z & \frac{1}{2}\chi^{(2)}E_y \\ \frac{1}{2}\chi^{(2)}E_z & \varepsilon_y & \frac{1}{2}\chi^{(2)}E_x \\ \frac{1}{2}\chi^{(2)}E_y & \frac{1}{2}\chi^{(2)}E_x & \varepsilon_z \end{bmatrix} \begin{bmatrix} E_x \\ E_y \\ E_z \end{bmatrix}, \tag{1}$$

in which E_j and D_j respectively refer to as the electric field and displacement field components. From the form of (1) it is clear that for a pure TE-polarization ($E_x = E_z = 0$), the medium essentially sees no nonlinearity and thus behaves linearly. Therefore, a pure TE-mode remains unchanged, as the substitution shows

$$\begin{bmatrix} 0 \\ D_y \\ 0 \end{bmatrix} = \begin{bmatrix} \varepsilon_x & 0 & \frac{1}{2}\chi^{(2)}E_y \\ 0 & \varepsilon_y & 0 \\ \frac{1}{2}\chi^{(2)}E_y & 0 & \varepsilon_z \end{bmatrix} \begin{bmatrix} 0 \\ E_y \\ 0 \end{bmatrix} = \begin{bmatrix} \varepsilon_x & 0 & 0 \\ 0 & \varepsilon_y & 0 \\ 0 & 0 & \varepsilon_z \end{bmatrix} \begin{bmatrix} 0 \\ E_y \\ 0 \end{bmatrix}. \tag{2}$$

But the situation for TM-polarization ($E_y = 0$) is different as shown below

$$\begin{bmatrix} D_x \\ D_y \\ D_z \end{bmatrix} = \begin{bmatrix} \varepsilon_x & \frac{1}{2}\chi^{(2)}E_z & 0 \\ \frac{1}{2}\chi^{(2)}E_z & \varepsilon_y & \frac{1}{2}\chi^{(2)}E_x \\ 0 & \frac{1}{2}\chi^{(2)}E_x & \varepsilon_z \end{bmatrix} \begin{bmatrix} E_x \\ 0 \\ E_z \end{bmatrix} = \begin{bmatrix} \varepsilon_x & 0 & 0 \\ \frac{1}{2}\chi^{(2)}E_z & \varepsilon_y & \frac{1}{2}\chi^{(2)}E_x \\ 0 & 0 & \varepsilon_z \end{bmatrix} \begin{bmatrix} E_x \\ 0 \\ E_z \end{bmatrix}. \tag{3}$$

Here, despite the TE E_y component is initially zero, D_y is not. Therefore, the energy is partially transferred to the TE-polarization and the presence of TM-components, even with no initial TE-field, leads to the excitation of TE-mode, which usually carries the second-harmonic. This fact has been experimentally shown to be true [29]. Therefore, $\chi^{(2)}$ nonlinear materials are not polarization conserving.

Now we consider simple $\chi^{(3)}$ nonlinear materials with the constitutive relation

$$\begin{bmatrix} D_x \\ D_y \\ D_z \end{bmatrix} = \begin{bmatrix} \varepsilon_x + \chi^{(3)}|\mathbf{E}|^2 & 0 & 0 \\ 0 & \varepsilon_y + \chi^{(3)}|\mathbf{E}|^2 & 0 \\ 0 & 0 & \varepsilon_z + \chi^{(3)}|\mathbf{E}|^2 \end{bmatrix} \begin{bmatrix} E_x \\ E_y \\ E_z \end{bmatrix}, \tag{4}$$

where $|\mathbf{E}|^2 = |E_x|^2 + |E_y|^2 + |E_z|^2$ is the local intensity of the electric field. Here, the diagonal nature of the nonlinear permittivity tensor shows that the TE- and TM-polarizations respectively obey

$$\begin{bmatrix} 0 \\ D_y \\ 0 \end{bmatrix} = \begin{bmatrix} \varepsilon_x + \chi^{(3)}|E_y|^2 & 0 & 0 \\ 0 & \varepsilon_y + \chi^{(3)}|E_y|^2 & 0 \\ 0 & 0 & \varepsilon_z + \chi^{(3)}|E_y|^2 \end{bmatrix} \begin{bmatrix} 0 \\ E_y \\ 0 \end{bmatrix}, \tag{5}$$

and

$$\begin{bmatrix} D_x \\ 0 \\ D_z \end{bmatrix} = \begin{bmatrix} \varepsilon_x + \chi^{(3)}\left(|E_x|^2 + |E_z|^2\right) & 0 & 0 \\ 0 & \varepsilon_y + \chi^{(3)}\left(|E_x|^2 + |E_z|^2\right) & 0 \\ 0 & 0 & \varepsilon_z + \chi^{(3)}\left(|E_x|^2 + |E_z|^2\right) \end{bmatrix} \begin{bmatrix} E_x \\ 0 \\ E_z \end{bmatrix}. \tag{6}$$

Hence, the simple $\chi^{(3)}$ nonlinear materials are polarization-preserving, in the sense that pure TE-modes or pure TM-modes remain unchanged and uncoupled.

But the important feature of $\chi^{(3)}$ nonlinear materials as can be inferred from (3), is that TE- and TM-polarizations, when both are present at the same time, can exchange energy through the intensity $|\mathbf{E}|^2$ term in the constitutive relation. This polarization coupling concept is not novel; however, its application to PC structures and experimental demonstration thereof has not been covered previously. For example, in a study by Zitelli et al. [39], the implementation of all-optical NOR gates based on the nonlinear interaction between orthogonal polarizations was proposed and discussed. In a

subsequent paper [40], the authors demonstrated the feasibility of the basic logic operations OR, AND, and NOT using nonlinear beam-propagation simulations. Another paper [41] discussed the usage of semiconductor slab waveguides as possible candidates for all-optical logic operations. More recently [42,43], various logic operations based on nonlinear interaction of fundamental transverse electric and magnetic polarizations have been proposed.

Chapter 3
Nonlinear Finite-Difference Time-Domain

In order to properly treat the implementation of an all-optical logic device, the theory governing the device operation must be analyzed. The theoretical basis for unidirectional energy transfer between orthogonal polarizations in planar PC waveguides is discussed in the next section. Also discussed is the theory behind the nonlinear FDTD code used to simulate these devices, as well as a description of its implementation. In the following section (2.2), the simulation results achieved thus far are presented, concluding with a list of the remaining structures that must be investigated.

The 2D FDTD method we developed is based on a modification of the original Yee's FDTD algorithm [35]. The original FDTD approach solves the coupled linear Maxwell's equations in differential form

$$\frac{\partial}{\partial t}\mathbf{H} = -\frac{1}{\mu}\nabla \times \mathbf{E}, \tag{7}$$

$$\frac{\partial}{\partial t}\mathbf{E} = +\frac{1}{\varepsilon}\nabla \times \mathbf{H}, \tag{8}$$

where the permittivity ε and the magnetic permeability μ are both time independent scalars. By discretizing the simulation domain into a finite computational grid, the magnetic and electric fields are computed at interlacing time intervals, as shown here for the x components

$$\begin{aligned} H_x{}^{n+\frac{1}{2}}(i, j+\tfrac{1}{2}, k+\tfrac{1}{2}) &= H_x{}^{n-\frac{1}{2}}(i, j+\tfrac{1}{2}, k+\tfrac{1}{2}) \\ &+ \frac{\Delta t}{\mu}\left(\frac{E_y^n(i, j+\tfrac{1}{2}, k+1) - E_y^n(i, j+\tfrac{1}{2}, k)}{\Delta z} - \frac{E_z^n(i, j+1, k+\tfrac{1}{2}) - E_z^n(i, j, k+\tfrac{1}{2})}{\Delta y} \right), \end{aligned} \tag{9}$$

$$E_x^{\,n+1}(i+\tfrac{1}{2},j,k) = E_x^{\,n}(i+\tfrac{1}{2},j,k)$$
$$-\frac{\Delta t}{\varepsilon}\left(\frac{H_y^n(i+\tfrac{1}{2},j,k+\tfrac{1}{2})-H_y^n(i+\tfrac{1}{2},j,k-\tfrac{1}{2})}{\Delta z}-\frac{H_z^n(i+\tfrac{1}{2},j+\tfrac{1}{2},k)-H_z^n(i+\tfrac{1}{2},j-\tfrac{1}{2},k)}{\Delta y}\right), \quad (9)$$

where n represents the time index, Δt is the timestep, Δy and Δz are the grid spacings in the y and z directions, respectively, and i, j, and k are the grid coordinates in the respective x, y, and z directions. The y and z field components are calculated from similar equations, with the spatial orientations of these field components as shown in Figure 1, commonly referred to as the Yee's cell.

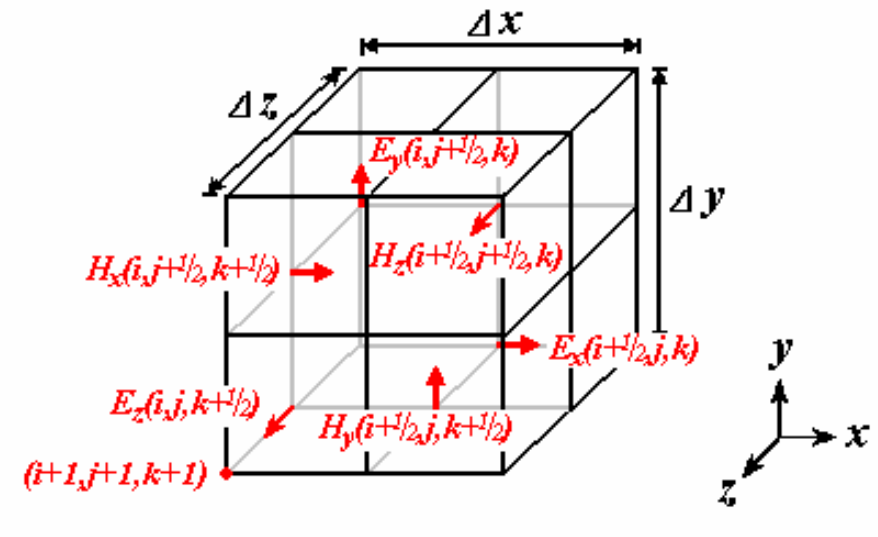

Figure 1. Traditional Yee's cell for FDTD field components.

In our nonlinear version, the first set of equations (Eq. (3)) is retained while the second set of equations is written as

$$D_x^{n+1}(i+\tfrac{1}{2},j,k) = D_x^{n}(i+\tfrac{1}{2},j,k) - \Delta t\left(\frac{H_y^n(i+\tfrac{1}{2},j,k+\tfrac{1}{2}) - H_y^n(i+\tfrac{1}{2},j,k-\tfrac{1}{2})}{\Delta z} - \frac{H_z^n(i+\tfrac{1}{2},j+\tfrac{1}{2},k) - H_z^n(i+\tfrac{1}{2},j-\tfrac{1}{2},k)}{\Delta y}\right), \quad (10)$$

where D_{x^n} is the electric displacement in the x direction, which is known through the nonlinear constitutive relation $\mathbf{D}^n = f\left(\mathbf{E}^n\right)\left(\mathbf{E}^n\right)$ (f here represents a function). After finding $\mathbf{D}^{n+1}$, the electric field is advanced from the inverse constitutive relation, i.e. $\mathbf{E}^{n+1} = f^{-1}\left(\mathbf{D}^{n+1}\right)\left(\mathbf{D}^{n+1}\right)$. This inversion process is possible either through exact analytical methods or an iterative approach starting with $\mathbf{E}^n$ as the initial value.

Although the $\chi^{(3)}$ susceptibility is generally a third-rank tensor, for a wide variety of materials (such as many of the semiconductors used in modern optoelectronics) most of the tensor elements are negligible or equal to each other due to material symmetries and other considerations. Therefore, the total number of independent tensor elements is significantly reduced. Many materials used in nonlinear optics have nonlinear susceptibilities that can be treated as a scalar quantity; these are the materials treated by this study. Some examples of $\chi^{(3)}$ materials of interest include most semiconductors including gallium arsenide, KD*P, and liquid crystals. Note that there are nonlinear algorithms which are capable of treating tensors [44], however these more complex methods have been developed for systems that require the full tensor forms, and do not provide significant benefits for materials such as those used for practical PC applications.

For simple, non-dispersive $\chi^{(3)}$ nonlinear materials, the required time-dependent (since **E** is a function of time) tensors can be actually found from the equivalent constitutive relation given by

$$\mathbf{D} = \varepsilon_0 \begin{bmatrix} \varepsilon_r + \chi^{(3)}|\mathbf{E}|^2 & 0 & 0 \\ 0 & \varepsilon_r + \chi^{(3)}|\mathbf{E}|^2 & 0 \\ 0 & 0 & \varepsilon_r + \chi^{(3)}|\mathbf{E}|^2 \end{bmatrix} \mathbf{E}. \tag{11}$$

Although this relation takes a more elaborate tensor form in the most general case, this compact notation is both mathematically consistent for the simple materials of interest and also convenient for the rest of this discussion. For self-focusing $\chi^{(3)}$ nonlinear media where the nonlinear polarization term is essentially a scalar, an inversion function $g = f^{-1}$ may be found in closed form using algebraic techniques, which after simplification results in

$$g\left(\varepsilon_r, \chi^{(3)}, D\right) = \frac{-\sqrt[3]{12}\varepsilon_r + \left(9\sqrt{\chi^{(3)}}D + \sqrt{12{\varepsilon_r}^3 + 81\chi^{(3)}D^2}\right)^{\frac{2}{3}}}{\sqrt[3]{18\left(9\sqrt{\chi^{(3)}}D + \sqrt{12{\varepsilon_r}^3 + 81\chi^{(3)}D^2}\right)}D\sqrt{\chi^{(3)}}}, \tag{12}$$

in which $D = |\mathbf{D}|$ (i.e. the magnitude of vector **D**) and ε_r is the local relative permittivity of the medium. Using the above expression, exact evaluation of the inverse constitutive relation becomes possible and the efficiency of the algorithm is improved by about 30% as compared with the comparable iterative approach. Although the exact improvement in efficiency will depend on computer architecture, programming language, etc., this approach in general will be equal to or faster than the one based on iteration, since at least one iteration that involves roughly the same number of calculations as Eq. (12) must be performed for each grid point during each time step.

In our algorithm, the frequency dependence of the third order nonlinear coefficient is ignored. This assumption is well justified if the optical frequency is far from the absorption resonance of the nonlinear materials [45]. Furthermore, the frequency

bandwidth of the optical signals is typically much smaller than the dispersion of the nonlinear coefficients, which allows us to treat the $\chi^{(3)}$ coefficient as a frequency independent constant.

Since the algorithm simulates the behavior of a nonlinear system, the absolute amplitude of the electromagnetic wave in our simulation carries physical meaning and cannot be normalized arbitrarily. A normalization factor $A_{I,N}$ is introduce which relates the physical electric field E and the normalized electric field E_N as $E_N = E/\sqrt{A_{I,N}}$. The material $\chi^{(3)}$ nonlinear coefficient is normalized as:

$$\chi_N^{(3)} = \chi^{(3)} A_{I,N} = n_2 \frac{cn_0^2}{\pi} A_{I,N}\,, \tag{13}$$

where n_0 is the linear refractive index, n_2 is the second-order nonlinear refractive index, and $\chi_N^{(3)}$ represents the normalized $\chi^{(3)}$ nonlinear coefficient. This renormalization is necessary to prevent the numerical values from approaching the upper or lower precision limits for a given computer architecture. The numerical results given by the FDTD correspond to the normalized values, which can be converted into physical values by using the appropriate normalization factor $A_{I,N}$. Also, according to Eq. (13) the normalized nonlinearity coefficient is directly related to the both the physical nonlinearity strength and the normalization factor. Thus, materials of various nonlinear strengths or different input intensity levels may be simulated by choosing appropriate values of the normalized nonlinearity strength. As an example of how physical nonlinear values compare with the corresponding normalized quantities, a value of $1.59*10^{-13}$ cm^2/W for n_2 (i.e. GaAs [46]) with $A_{I,N} = 1$ corresponds to a normalized $\chi^{(3)}$ of $5.5*10^{-15}$.

The FDTD implementation was coded for two-dimensional simulations with rectangular computational domains. At the four computational boundaries, either periodic Bloch [47], perfectly matched layer (PML) [48], or a combination of the two boundary conditions can be specified, depending on the dielectric structure under consideration. The developed code was written in C running under a Tcl/Tk shell on a Linux platform. The efficiency of the nonlinear version, defined as the computation time for a given structure, is measured to be roughly half that of the original linear version. The basic method is similar to that of Tran [38], who developed a simpler 1-D code for $\chi^{(3)}$ materials.

It can be shown that Yee's FDTD algorithm is stable under the Courant's stability condition [49], asserting that the numerical propagation velocity must be greater than the maximum phase velocity of the light in the structure [50]

$$\frac{1}{\Delta t\sqrt{(\Delta x)^{-2}+(\Delta z)^{-2}}} \geq \sup\left\{\frac{1}{\sqrt{\mu_0\varepsilon_0\varepsilon_r}}\right\} = c_{\max}\,. \tag{14}$$

Notice that this derivation is performed for the two-dimensional case. This condition is both necessary and sufficient for numerical stability in a FDTD code that only considers linear effects. The extension to anisotropic materials has an almost identical stability condition

$$\frac{1}{\Delta t\sqrt{(\Delta x)^{-2}+(\Delta z)^{-2}}} \geq \sup\left\{\frac{1}{\sqrt{\mu_0\varepsilon_0\left|\mathrm{eig}\{\overline{\overline{\varepsilon}}_r\}\right|}}\right\} = c_{\max}\,, \tag{15}$$

except that now the eigenvalues of the permittivity tensor $\overline{\overline{\varepsilon}}_r$ are considered in the expression.

In order to examine the stability of the nonlinear FDTD implementation, suppose the simulation is run for a given time-step and spatial grid size, and the output field is observed over the entire structure. Assuming that the input field is kept unchanged, the simulation must produce the same results as if the time-dependent linear system were solved with the permittivity being a suitably defined anisotropic time-dependent tensor, rather than the original nonlinear case. This is because in Maxwell equations for anisotropic media (and therefore the FDTD method also), field components can be decomposed into a superposition of plane waves along various directions. Each direction is normally associated with two eigenvalues and two eigenvectors, which characterize the corresponding eigenmodes. Generally, these two modes propagate at different phase velocities, and if for each direction the fast mode is stabilized in the numerical scheme, so would be the slower mode. It can be easily demonstrated that the fastest propagating wave corresponds to the smallest refractive index, which must be one of the eigenvalues of the refractive index matrix of the anisotropic medium [51]. Therefore it is sufficient to consider only the eigen-indices.

For $\chi^{(3)}$ nonlinearity the constitutive relationship, i.e. Eq. (11), depends on the strength of the electric field at each grid point in the computation space, which makes the stability analysis more complicated than the linear or simple anisotropic cases. The $\chi^{(3)}$ materials of interest are mainly self-focusing media and the corresponding tensor is isotropic. An analysis of the minimum value taken by the eigenvalues of the constitutive matrix shows that for any positive values of $\chi^{(3)}$ (i.e. for any positive Kerr materials), Courant's stability condition is still sufficient for code stability

$$\min\left\{\mathrm{eig}\left\{\overline{\overline{\varepsilon}}\right\}\right\} = \varepsilon_r + \chi^{(3)}\left|\mathbf{E}\right|^2 \geq \varepsilon_r, \quad \chi^{(3)} \geq 0. \tag{16}$$

Therefore, the linear stability condition is applicable, since the self-focusing effect results in a local decrease of phase velocity. As verification of this statement, a more detailed calculation for the scalar TE modes in self-focusing media may be performed [52] which results in

$$\frac{\sqrt{\frac{\partial\left[\varepsilon_r E + \chi^{(3)} E^3\right]}{\varepsilon_r \partial E}}}{\Delta t\sqrt{(\Delta x)^{-2} + (\Delta z)^{-2}}} \geq \frac{1}{\Delta t\sqrt{(\Delta x)^{-2} + (\Delta z)^{-2}}} \geq c_{\max}. \tag{17}$$

Clearly, the same result is reached, confirming that Courant's stability condition is sufficient for $\chi^{(3)}$ nonlinearity in the materials of interest in which only one independent $\chi^{(3)}$ component exists.

Chapter 4
Simulation Results

4.1 Verification of Nonlinear $\chi^{(3)}$ Code

In order to validate the nonlinear FDTD code developed in the previous sections, the well-understood nonlinear optical phenomenon of self-phase modulation in $\chi^{(3)}$ media was used. The index of refraction n is the square root of the permittivity, which in this case may be written as

$$n = n_0 + \delta n = \sqrt{\varepsilon_r + \chi^{(3)}|\mathbf{E}|^2} \approx n_0 + \frac{\chi^{(3)}}{2\sqrt{\varepsilon_r}}|\mathbf{E}|^2, \tag{18}$$

where ε_r is the relative permittivity and n_0 is the linear refractive index. Self-phase modulation arises from the δn term, which changes the local effective index of the material in proportion to the square of the electric field strength.

If we consider a plane wave incident upon a material exhibiting third-order nonlinearity, we find that for a TE-polarized wave (i.e. electric field normal to the 2D computation plane, which is the x-y plane) the z-component of the electric field has the form

$$E_z = A\cos(kx + \phi) = A\cos(\omega n x + \phi), \tag{19}$$

where A is the amplitude, k is the wavenumber, ω is the angular frequency, x is the position along the propagation direction, and φ is a phase constant. Here, we normalize the speed of light in vacuum to $c = 1$. In our simulations, the unidirectional traveling wave excited by the Huygens source can be well approximated by a plane wave near the right end of the computational domain. If we neglect φ for the moment, which is valid as

long as the nonlinear field component is relatively weak, we can take the second derivative of E_z and approximately find

$$\begin{aligned} \frac{dE_z}{dx} &= -\omega n A \sin(\omega n x) \\ \frac{d^2E_z}{dx^2} &= -\omega^2 n^2 A \cos(\omega n x) \end{aligned} . \tag{20}$$

We may then divide the second derivative by the original field and take the square root and write

$$n = \sqrt{\frac{-\frac{d^2E_z}{dx^2}}{\omega^2 E_z}} . \tag{24}$$

Shifting of the calculated values due to the phase constant and discrete differentiation may be accounted for by considering the peaks of the numerator and denominator terms under the square root, as shown

$$n = \sqrt{\frac{\max\left(-\frac{d^2E_z}{dx^2}\right)}{\max\left(\omega^2 E_z\right)}} . \tag{21}$$

An additional issue that must be accounted for is the extra harmonic components present in E_z for the nonlinear case [54], which likely result from the fact that the spatial variation of the phase term φ can no longer be ignored when large values are chosen for $\chi^{(3)}$. The electric field in this case is not perfectly sinusoidal, resulting in considerable distortion of the calculated second derivative. This can be overcome by filtering the field values using a low-pass filter such that only the fundamental harmonic component remains.

Using Eq. (18), δn may now be calculated by subtracting the value of the linear refractive index from the refractive index obtained numerically from Eq. (21). Notice

that the maximum of the squared E_z values from the FDTD simulation results was used in the calculation, although the average value is assumed in the theoretical analysis; the average field intensity can be related to the maximum field intensity through:

$$\left\langle |\mathbf{E}|^2 \right\rangle = |\mathbf{E}|^2_{\max} / 2 . \tag{22}$$

Comparing the simulation results (Eq. (21)) with the analytical expression for n (Eq. (18)), we find agreement to within 12% error. We may also compare the permittivity values directly, eliminating the approximation used to separate the square-root term in Eq. (18). The values using this approach agree to within only 2.6% error, much smaller due to the fact that the error in truncation of the binomial expansion of Eq. (18) is no longer ignored. Since it is commonly understood that the FDTD in practical usage has a typical error of up to five percent, these results verify within reasonable agreement the accuracy of our third-order nonlinear code.

4.2 Polarization Coupling in Bulk Silicon

Several simulations were performed to evaluate the feasibility of the polarization interaction idea and to specify the design parameters necessary for a device based on this idea. The first simulation to demonstrate polarization mixing was for a simple slab waveguide composed of silicon (ε_r = 7.29) in air (ε_r = 1.0). Silicon is used here because of its relatively strong nonlinear refractive coefficient, n_2, of $4.5*10^{-14}$ cm^2/W [46]. It is also a popular material for planar photonics, due to its large refractive index (useful for nano-scale waveguides), transparency for optical communications wavelengths, and maturity of fabrication technology. The entire waveguide is assumed to be composed of $\chi^{(3)}$ nonlinear material, PML boundary conditions are used on all sides, and the power of

the TE and TM waves is calculated just before the source, just after the source, and at the end of the waveguide, as shown in Figure 2. The source was Huygens source with a Gaussian frequency spectrum centered at a normalized frequency of 0.509 and having

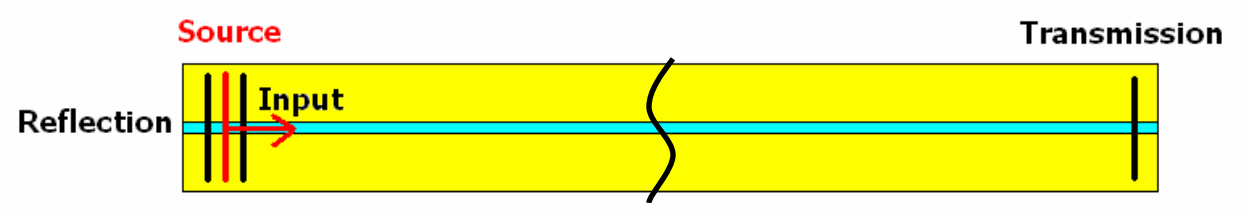

Figure 2. Diagram of slab waveguide showing computation regions used for power calculations.

both TE and TM components with equal amplitudes. The bandwidth of the Gaussian source was chosen to be 4% of the center frequency. The relatively large nonlinear values used are nonphysical, but are used to observe the effects of the nonlinear material without simulating a very large computational domain. The TE transmission spectrum of the nonlinear waveguide a few values of normalized $\chi^{(3)}$ is shown in Figure 3a, which show that the TE power actually decreases at the center frequency of the source for the nonlinear cases, rather than the increase that would be expected if the TM polarization was being converted to TE. The TM power (Figure 3b) also decreases, although obviously no power conversion is taking place. An

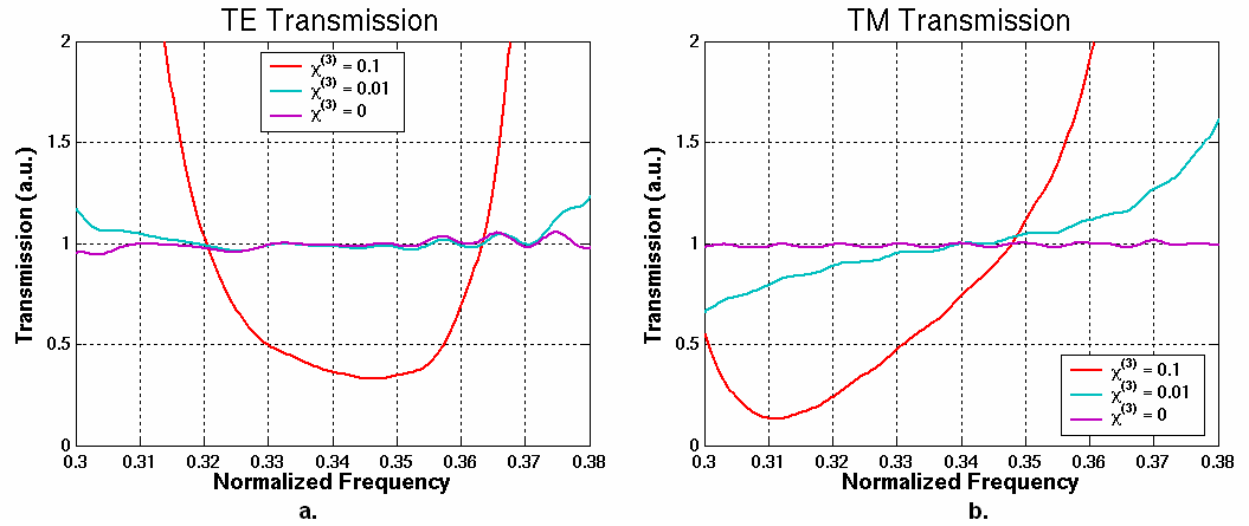

Figure 3a. Plot of transmission through slab waveguide shown in Figure 2 for TE polarization. b. TM polarization.

explanation is found by observing a larger frequency range as seen in Figure 4, where the power is now plotted on a log scale; a peak exists at the third harmonic of the source frequency, indicating that significant power is being converted to the third harmonic rather than TM to TE power conversion. This is due to the fact that both the TE and TM signals experience third harmonic generation and thus depletion at the pump wavelength, whereas the TM-to-TE conversion only produces gain for TE while further depleting the TM. The transmission spectra in Figure 4 corroborate this assertion, where peaks at the third-harmonic of the center frequency can be seen for both polarizations. Spectral broadening is also observed for the nonlinear cases as compared with the linear case.

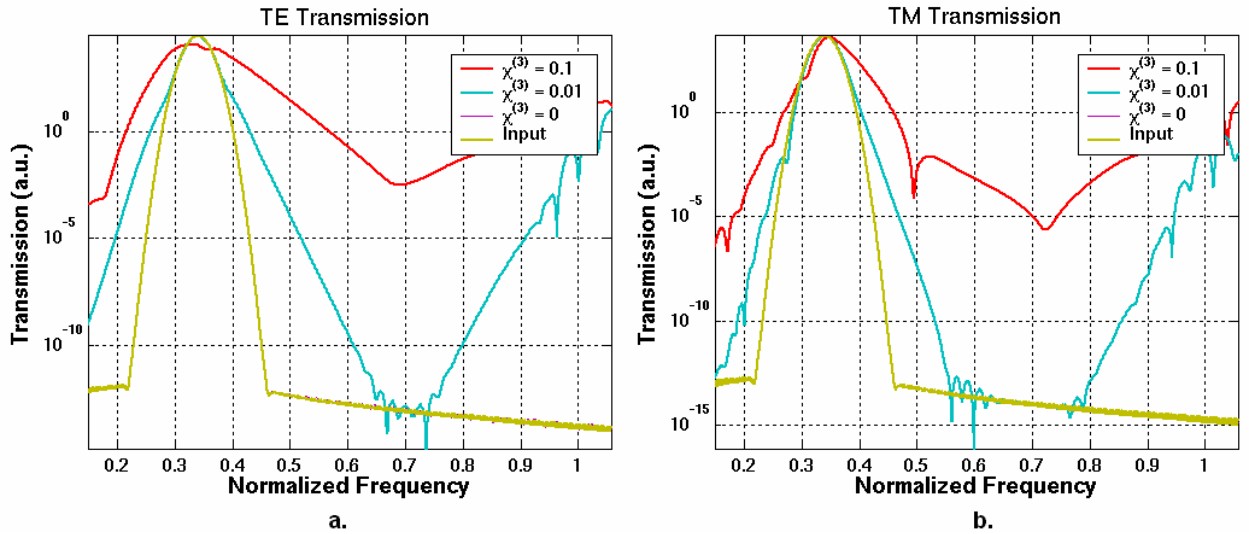

Figure 4a. Plot of transmission through slab waveguide shown in Figure 2 on a large frequency scale for TE polarization. b. TM polarization.

This results from self-phase modulation (SPM) arising from the Kerr-type nonlinearity, due to the dispersion of the waveguide. Although this dispersion is relatively small, the large nonlinear strengths used exaggerate the SPM effects.

Since the dominant third-harmonic conversion prevented the observation of cross polarization coupling in a slab waveguide, another optical device should that is better suited to the desired phenomenon. The photonic crystal waveguide (PCWG) can be as such a device, since its operation is governed by the bandgap of the PC and can inhibit the generation of frequencies within this forbidden range. As a defect-based device, such as a waveguide, guiding only occurs for frequencies within the bandgap of the PC; other frequencies are not well-confined and radiate evanescently into PC resulting is very large propagations loss. Thus, a triangular-lattice W1 PC waveguide (W1 denotes that the waveguide is formed by a single line-defect in the PC lattice) was simulated next (Figure 5), where the line-defect region of the waveguide is assumed to be composed of $\chi^{(3)}$ nonlinear material. The hole radius is 44% of the periodicity, the same refractive indices

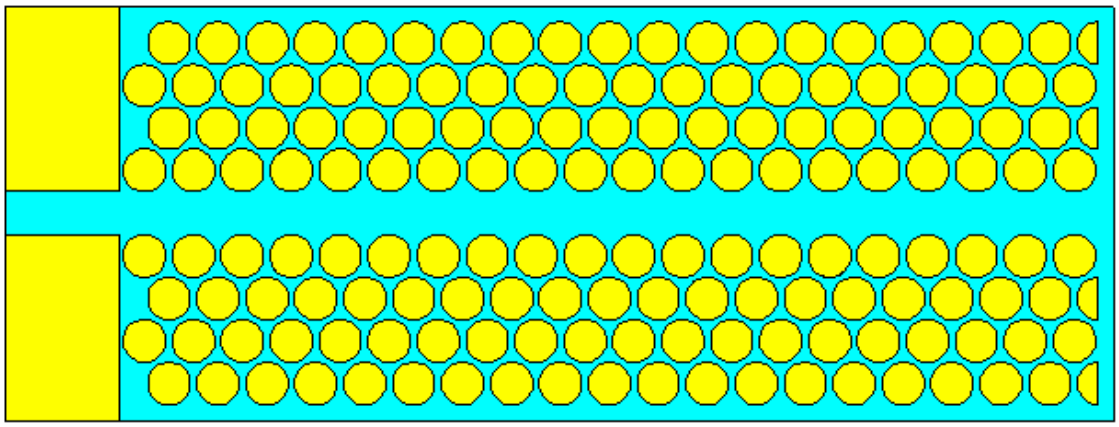

Figure 5. Diagram of triangular-lattice photonic crystal waveguide, where yellow indicates air and cyan indicates silicon.

were used as for the previous slab waveguide, and 36 grid points per PC period were used for the computational domain. The triangular-lattice geometry was used because of its large bandgap for the TM polarization, from 0.376 to 0.513 in normalized frequency (Figure 6), although the corresponding TE bandgap in the guiding direction is much smaller, from only 0.493 to 0.502 in normalized frequency.

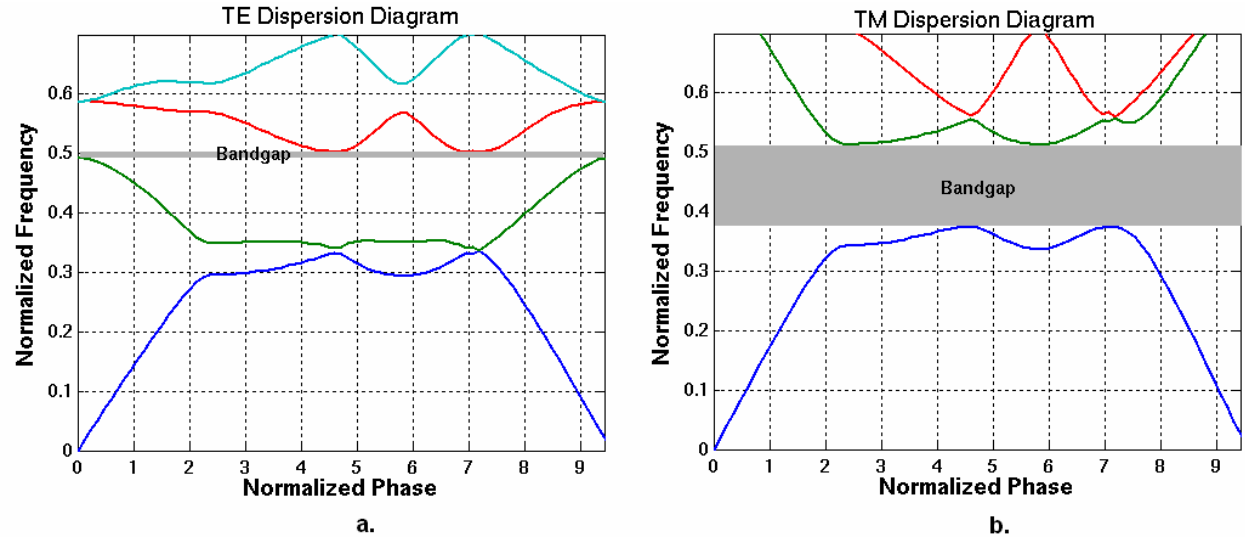

Figure 6a. Band diagram for triangular-lattice photonic crystal for TE polarization. b. TM polarization.

Here, some power transfer from TM to TE polarizations is seen (Figure 7), since the transmission exceeds 1.0 for normalized frequencies around 0.487 and lower, for normalized $\chi^{(3)} = 0.1$. The lack of significant change in the transmission for the TM cases

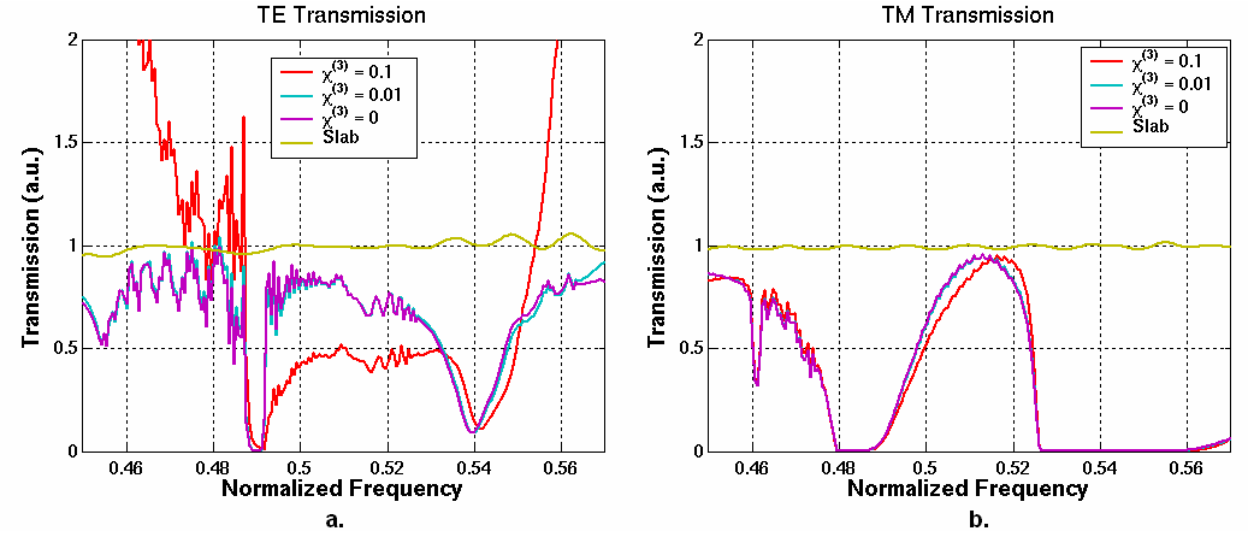

Figure 7a. Plot of transmission through photonic crystal waveguide shown in Figure 5 for TE polarization. b. TM polarization.

and for the smaller value of nonlinearity for TE indicates that the frequency-mixing effects seen for the slab waveguides have been largely suppressed. Unfortunately, the frequencies where the gain is observed for the TE polarization are outside the bandgap, and thus only weakly guided with likely large propagation loss into the PC cladding. However, this may be offset somewhat by the self-focusing effect of the nonlinear Kerr material of which the PC waveguide core is composed, which slightly improves the confinement of the light due to total internal reflection. The largest gain, at 0.487 in normalized frequency, is 3.0dB with compared to the linear PCWG transmission and 2.3dB as compared with the slab waveguide. Also, the SPM effects seen for the slab waveguide simulations are still present, as can be seen in Figure 8, which again shows the

non-normalized transmission on a log scale and for a wider range of frequencies. These figures, when compared with the corresponding plots for the slab waveguide, corroborate the assertion that the higher-harmonic effects have been reduced by the PC lattice.

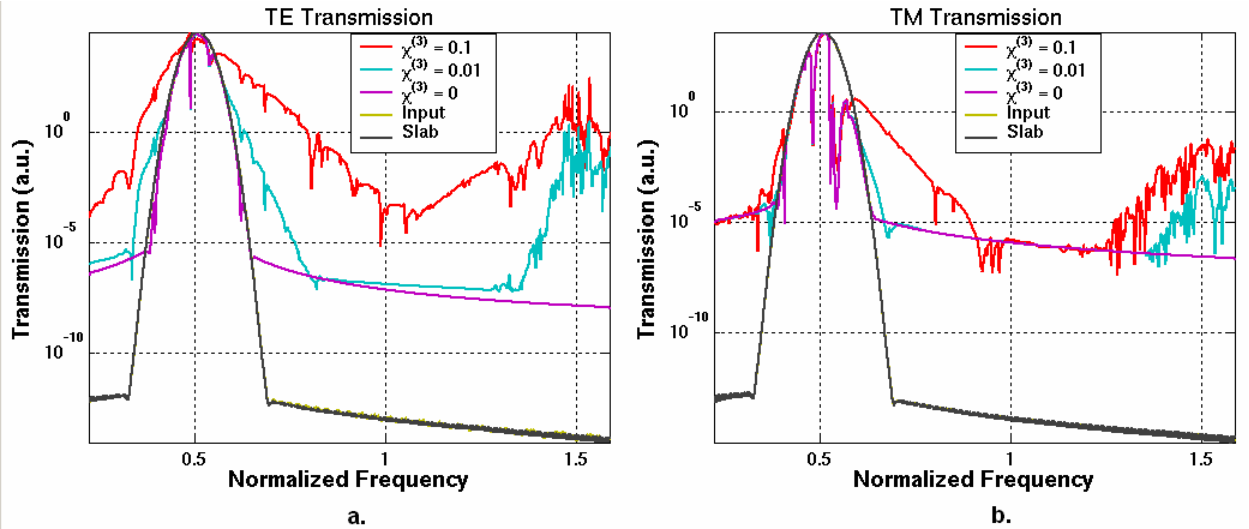

Figure 8a. Plot of transmission through photonic crystal waveguide shown in Figure 5 on a large frequency scale for TE polarization. b. TM polarization.

The coupled resonator optical waveguide (CROW) [55,56] is another device that may be used to increase the effects of nonlinear phenomena and coupling between co-propagating beams. In general, a CROW is a series of cavities placed close enough that light can propagate through the structure via evanescent coupling between adjacent resonators. Although a PC CROW design still relies on the bandgap for mode confinement and can suffer from DBR effects and the problem of overlapping bandgaps for both TE and TM polarizations, the reduced group velocity of its propagating modes translates into an effective enhancement of for nonlinear effects due to the "slow" light [33]. The CROW used here (Figure 9) is based on the same bulk PC as the previous PC waveguide, except that now the defect defining the guiding region is the elimination of

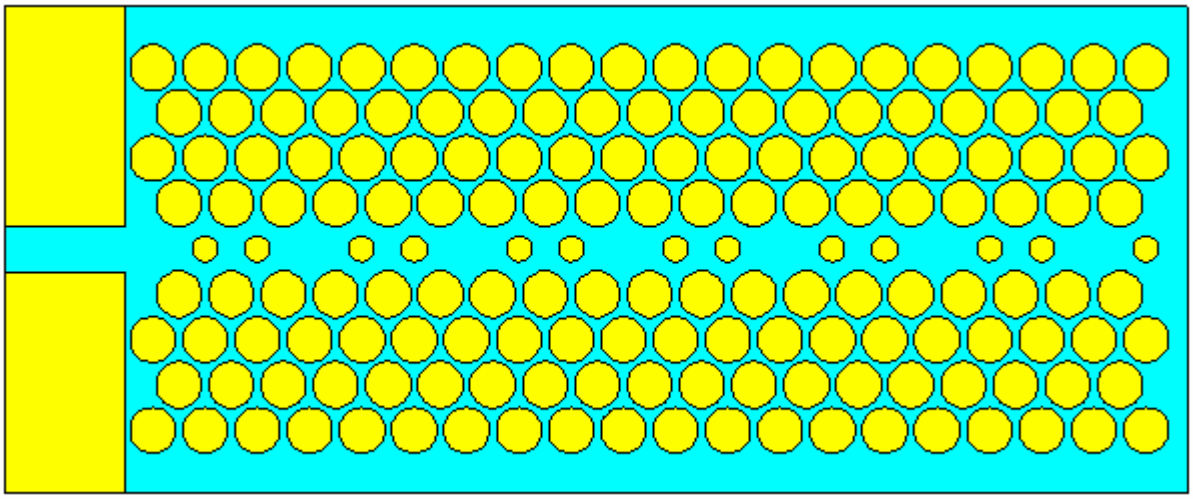

Figure 9. Diagram of photonic crystal coupled resonator optical waveguide, where yellow indicates air and cyan indicates silicon.

every third air hole in one row, rather than the entire row of holes. The mode dispersion for frequencies in the bandgap for TE and TM polarizations is shown in Figure 10, where the guided modes overlap at around 0.487 and again at 0.510 in normalized frequency. These frequencies are particularly interesting since the points where the modes overlap

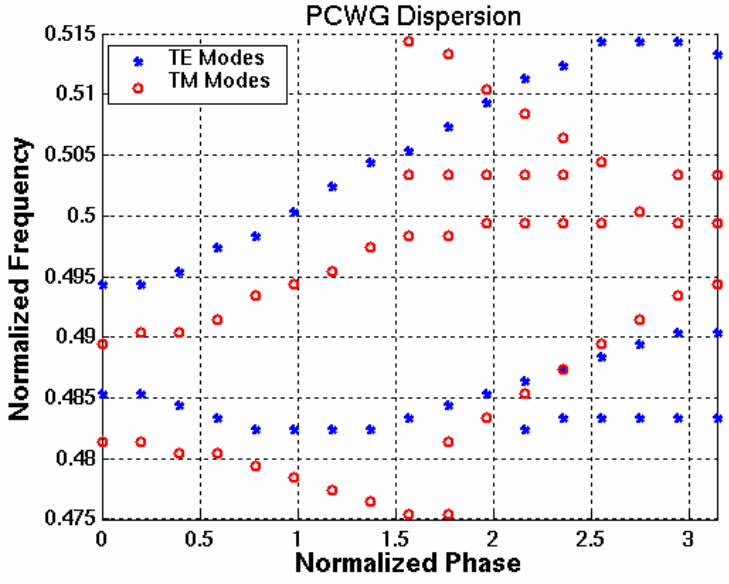

Figure 10. Dispersion diagram of coupled resonator optical waveguide shown in Figure 9 for TE and TM polarizations.

indicate where the optimal interaction between TE and TM modes should occur, due to phase matching. Also note the nearly flat slope of the dispersion curves, indicating a very small group velocity for the guided modes and thus a long interaction time and greater slow-light enhancement.

From Figure 11, transmission peaks can be seen for the TE polarization near the frequencies where the guided mode is predicted to overlap with the guided TM mode, although significant transmission is seen only at the lower frequency band for the TM

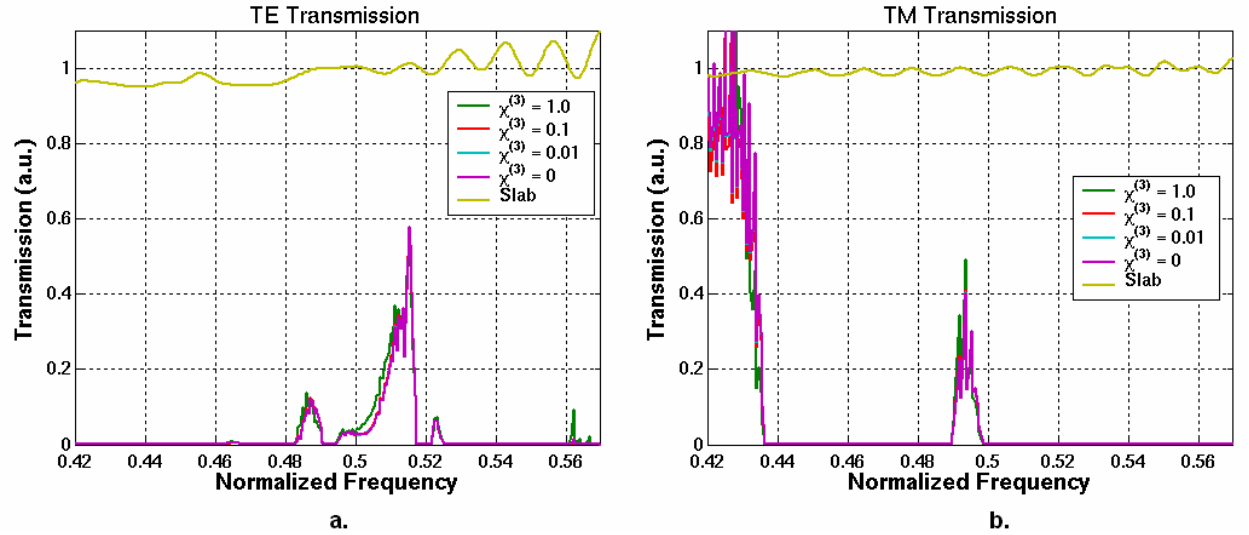

Figure 11a. Plot of transmission through coupled resonator optical waveguide shown in Figure 9 for TE polarization. b. TM polarization.

mode. Only very small gain is observed for the TE polarization, and although the nonlinear $\chi^{(3)}$ values used have been increased by an order of magnitude, the gain is still weaker than for the PCWG. This is due to the low transmission of the CROW itself, which limits the optical power and thus observable nonlinear effects for the guided modes. The maximum gain observed was only 1.26dB at normalized frequency 0.508, and the transmission at that frequency has dropped to 22%. However, one advantage of

the CROW design, as shown in the larger frequency scale transmission plot in Figure 12, is that the higher-order nonlinear effects are now almost completely suppressed.

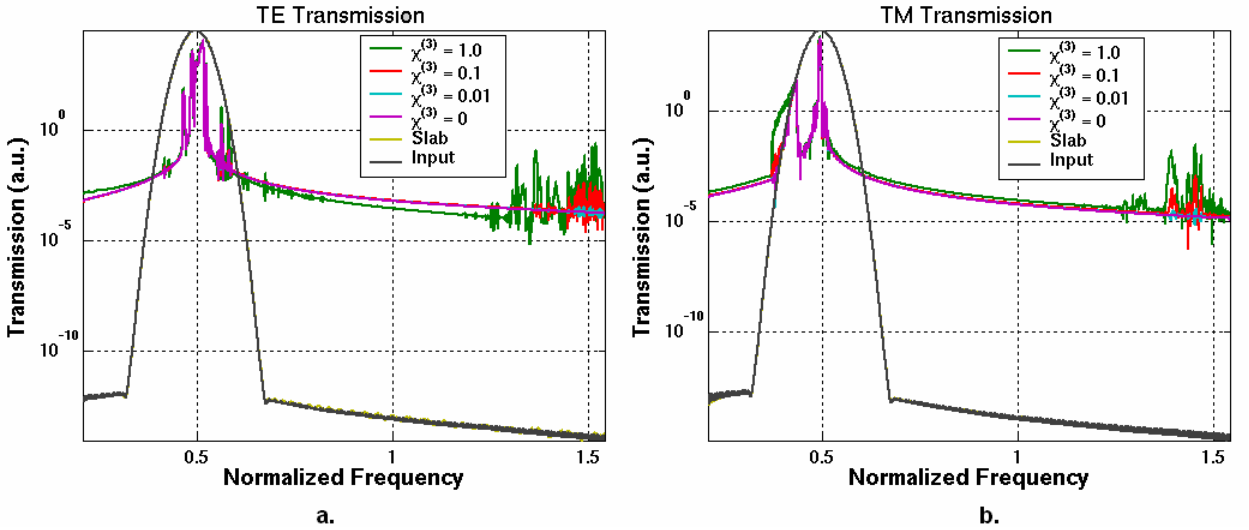

Figure 12a. Plot of transmission through coupled resonator optical waveguide shown in Figure 9 on a large frequency scale for TE polarization. b. TM polarization.

4.3 Polarization Coupling Using Nonlinear Polymer Infiltrates

Rather than relying on the nonlinear properties of bulk semiconductors such as silicon, as in the previous section, we can take advantage of the empty holes that constitute a PC by filling them with a nonlinear polymer material. These polymers offer a wide variety of characteristics, including extremely large nonlinear coefficients as compared with traditional semiconductors. This flexibility offered by nonlinear polymers has made them the focus of much research recently.

In order to maintain a large permittivity contrast when using polymer material systems, which often have permittivity values greater than that of air, the high-contrast material should have a larger permittivity. Thus, gallium arsenide, another semiconductor but with a larger a permittivity that silicon, is a good candidate. The simulations from the previous section were performed again using the same geometry,

but this time for a slab waveguide composed of gallium arsenide (ε_r = 12.96) in a background of nonlinear polymer (ε_r = 1.69).

The simulation results for the triangular-lattice PCWG using this new material system are shown next, where the TM bandgap is now shifted to 0.284 to 0.393 in normalized frequency; the TE bandgap is from 0.371 to 0.380. The transmission through the waveguide is shown in Figure 13, for valued of normalized $\chi^{(3)}$ now increased by two orders of magnitude. It is immediately obvious that the nonlinear effects are weaker in

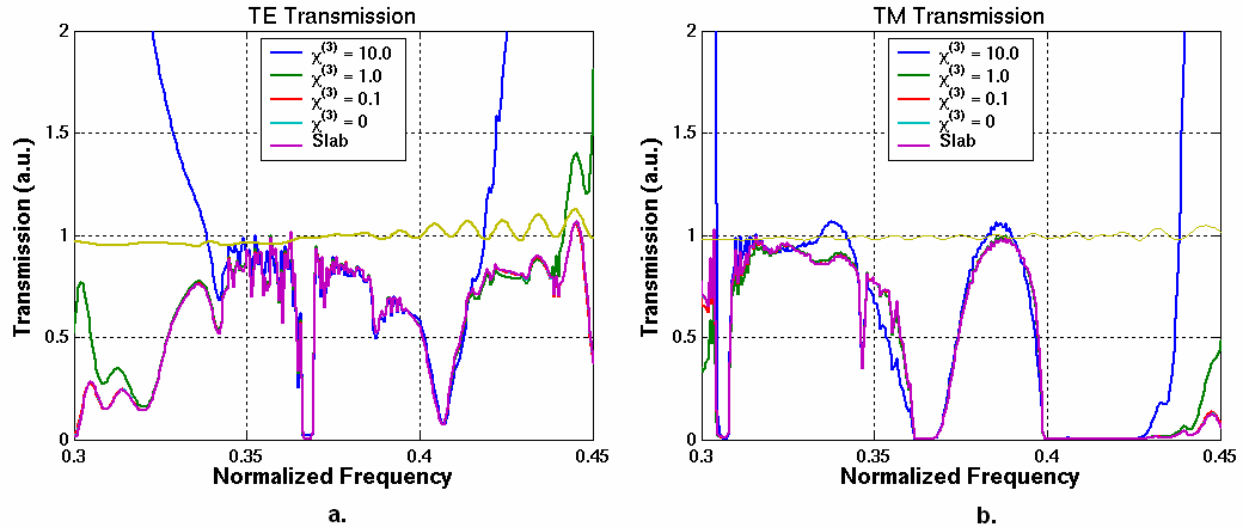

Figure 13a. Plot of transmission through polymer and gallium arsenide photonic crystal waveguide for TE polarization. b. TM polarization.

this structure, primarily due to the decreased amount of nonlinear material (only in the air hole regions) and the reduced interaction of the propagating energy with this material, since the majority of the energy in concentrated in the center of the defect guiding region and the first rows of air holes adjacent to this region [57,58]. However, there still appears to be small TE gain for frequencies in the range of 0.344 to 0.361, although not enough to be significant in this noisy transmission region. The plots showing a wider frequency

range in Figure 14 indicate that the third-harmonic nonlinear effects are again suppressed as compared with the slab waveguide. In addition, the SPM effects appear to be reduced

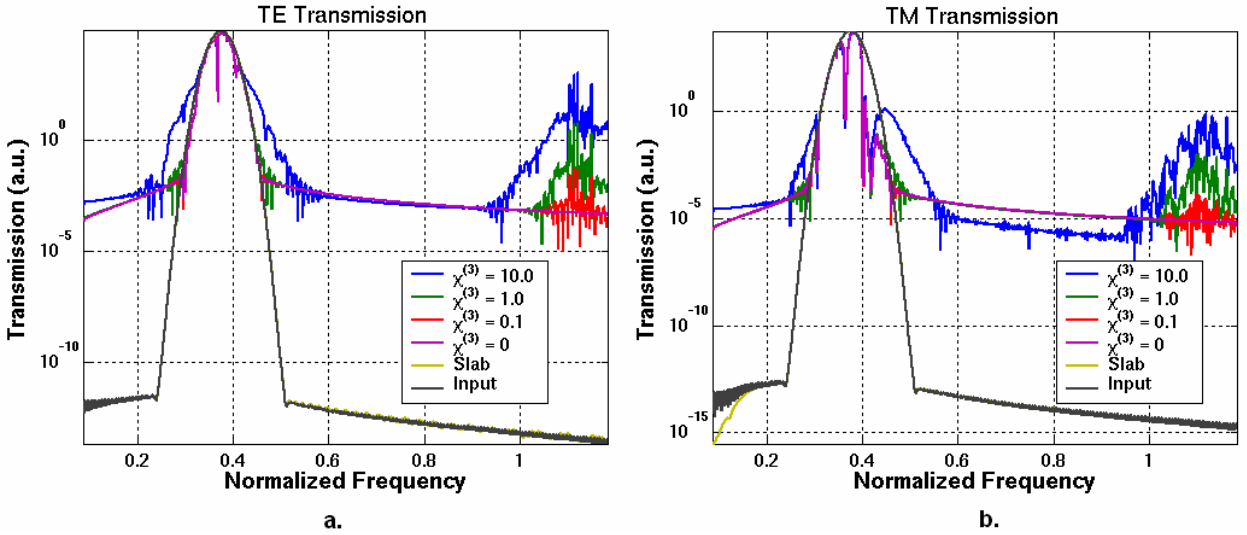

Figure 14a. Plot of transmission through polymer and gallium arsenide photonic crystal waveguide on a large frequency scale for TE polarization. b. TM polarization.

as compared to the previous PCWG simulations, although the maximum gain achieved suffers as well. Note that the transmission for a slab waveguide surround by a cladding of nonlinear material is very similar to the plots shown in Figures 3 and 4, again using normalized $\chi^{(3)}$ that are larger by two orders of magnitude.

Finally, the revised simulations were run for the PC CROW, which should provide better coupling to the nonlinear polymer via the filled holes in the high-intensity guiding region of the waveguide, in addition to the slow-light enhancement. The transmission results are shown on a log scale in Figure 15 for the same normalized $\chi^{(3)}$ values that were used with the PCW simulations. There appears to be a significantly wider transmission band as compared with the previous CROW structure (about 0.372 to 0.388 in

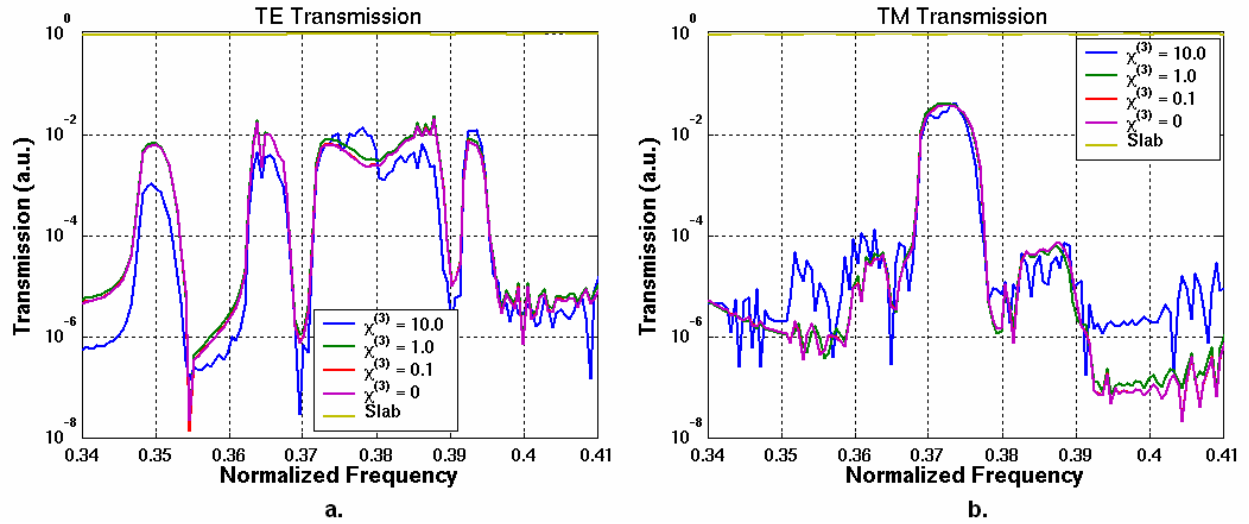

Figure 15a. Plot of transmission through polymer and gallium arsenide coupled resonator optical waveguide for TE polarization. b. TM polarization.

normalized frequency),although the overall transmission level is much lower. However, the apparent TE gain is almost as much as for the previous CROW structure for the normalized $\chi^{(3)} = 1.0$, and even larger for $\chi^{(3)} = 10.0$. In fact, the gain over the linear case at normalized frequency 0.378 is 7.4dB, although the transmission is only 1.4%. The transmission over a larger frequency span, shown in Figure 16, demonstrates that practically all of the higher-order frequency mixing effects have been eliminated. Also, the SPM has been minimized, due largely to the lower intensity of light in the nonlinear material. Since this inhibition of the third-harmonic is so dramatic even for the larger values of normalized $\chi^{(3)}$ used, it is likely that by manipulating the tradeoff between transmission and higher-frequency suppression, a CROW structure may found that exhibits higher transmission at the fundamental frequency and stronger TE to TM polarization conversion, while maintaining the strong suppression of the higher harmonics.

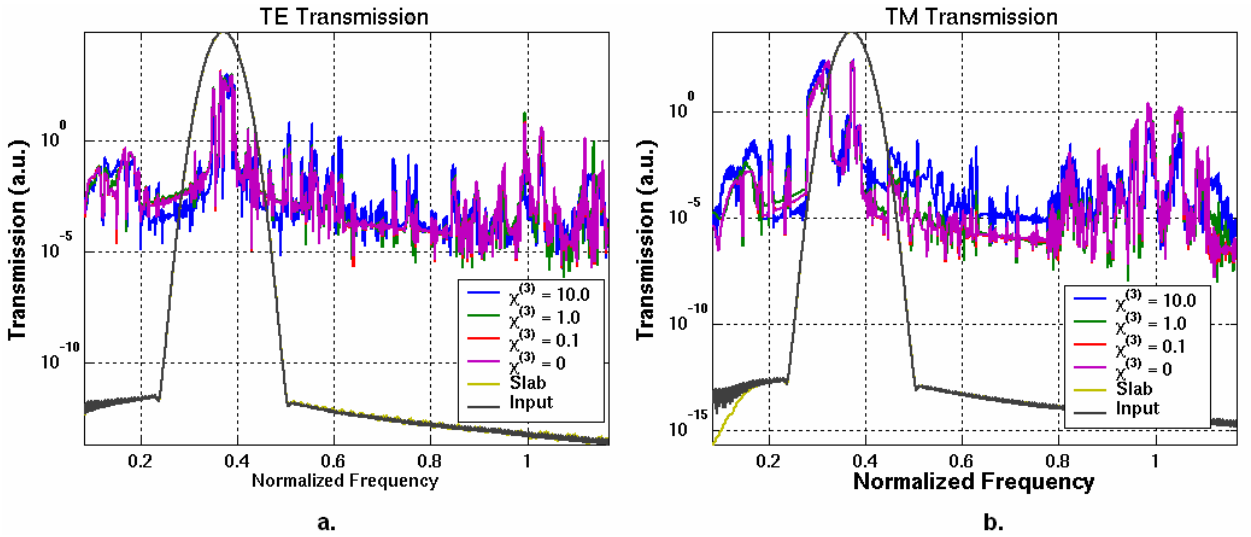

Figure 16a. Plot of transmission through polymer and gallium arsenide coupled resonator optical waveguide on a large frequency scale for TE polarization. b. TM polarization.

Chapter 5
Conclusions

The idea of coupling between orthogonal polarizations in the presence of a simple nonlinear $\chi^{(3)}$ material has been presented. This concept relies on the intrinsic nature of the constitutive relationship for this type of nonlinear materials. Combined with a framework for all-optical logic, this nonlinear coupling combined with PC structures could form the basis for basic on-chip nano-photonic computing functionality.

A 2D FDTD code has been presented that incorporates an efficient model of third-order nonlinear effects that does not require iteration or matrix inversion techniques. The explicit formulation increased the computation efficiency by as much as 30% over the iterative technique. This simulation tool is stable under Courant's criteria without the requirement of any extra constraints beyond that of the linear FDTD method. Also, nonlinear strengths of any value can be simulated, and a direct relationship equates the normalized quantity used in the computation to real-world values of nonlinear refractive index and optical intensity. The FDTD code was verified numerically using the analytical theory describing the well-studied phenomenon of self-phase modulation. The phase shift calculated from the simulation results agreed with theory to within 2.6%. Thus, it is capable of simulating Kerr-type nonlinear effects with accuracy equal to or greater than that of the FDTD technique itself.

Finally, the concept of TM to TE polarization coupling was been demonstrated in PCWGs and PC-based CROWs. The case of the guiding semiconductor material having nonlinear properties was considered, as well as that of the holes of the PC being infused with a nonlinear polymer. Suppression of undesirable higher-order $\chi^{(3)}$ effects was in the

PC structures was shown, allowing for TE gain from polarization coupling within a limited bandwidth. Peak gain values of 3.0dB for normalized $\chi^{(3)} = 0.1$ in a PCWG and 7.0dB for normalized $\chi^{(3)} = 10.0$ in a polymer-infused CROW were observed. These preliminary results demonstrate the validity of this concept and suggest that under optimization it should be possible to achieve gain figures that are suitable for the implementation of active photonic functionalities.

References

1. R. W. Boyd, *Nonlinear Optics*, San Diego, CA: Academic Press, Inc., 1992.

2. Y. S. Kivshar and G. Agrawal, *Optical Solitons: From Fibers to Photonic Crystals*, Boston, MA: Academic Press, Inc., 2003.

3. C. Flytzanis and J. L. Oudar, *Nonlinear Optics: Materials and Devices*, Berlin: Springer Verlag, 1986.

4. D. L. Mills, *Nonlinear Optics, 2nd Ed.*, Berlin: Springer Verlag, 1998.

5. A. Bhardwaj, "All-optical logic circuits based on polarization properties of nondegenerate four-wave mixing," J. Opt. Soc. Am. B, vol. 18, pp. 657-665, 2001.

6. A. Bhardwaj, P. O. Hedekvist, K. Vahala, "Erratum: All-optical logic circuits based on polarization properties of nondegenerate four-wave mixing," *J. Opt. Soc. Am. B*, vol. 18, p. 1956, 2001.

7. P. O. Hedekvist, A. Bhardwaj, K. Vahala, "Advanced all-optical logic gates on a spectral bus," *Appl. Opt.*, vol. 40, p. 1761-1766, 2001.

8. S. G. Johnson, S. Fan, P. R. Villeneuve, J. D. Joannopoulos, and L. A. Kolodziejski, "Guided modes in photonic crystal slabs," *Phys. Rev. B*, vol. 60, no. 8, pp. 5751-5758, 1999.

9. M. Qiu, K. Azizi, A. Karlsson, M. Swillo, and B. Jaskorzynska, " Numerical studies of mode gaps and coupling efficiency for line-defect waveguides in two-dimensional photonic crystals," *Phys. Rev. B*, vol. 64, no. 15, pp. 155113-155117, 2001.

10. S. Boscolo, C .Conti, M. Midrio, and C. G. Someda, "Numerical analysis of propagation and impedance matching in 2D photonic crystal waveguides with finite length," *J. Lightwave Technol.*, vol. 20, no. 2, pp. 304–310, 2002.

11. P. Lalanne, "Electromagnetic analysis of photonic crystal waveguides operating above the light cone," *IEEE J. Quantum Electron.*, vol. 38, no. 7, pp. 800–804, 2002.

12. T. Sondergaard, J. Arentoft, and M. Kristensen, "Theoretical analysis of finite-height semiconductor-on-insulator-based planar photonic crystal waveguides," *J. Lightwave Technol.*, vol. 20, no. 8, pp. 1619–1626, 2002.

13. E. Lidorikis, M. L. Povinelli, S. G. Johnson, and J. D. Joannopoulos, "Polarization-independent linear waveguides in 3D photonic crystals," *Phys. Rev. Lett.*, vol. 91, no. 2, pp. 23902-23905, 2003.

14. E. Yablonovitch, “Inhibited spontaneous emission in solid-state physics and electronics,” *Phys. Rev. Lett.*, vol. 58, no. 20, pp. 2059–2062, 1987.

15. S. John, “Strong localization of photons in certain disordered dielectric superlattices,” *Phys. Rev. Lett.*, vol. 58, no. 23, pp. 2486–2489, 1987.

16. K. M. Ho, C. T. Chan, and C. M. Soukoulis, “Existence of a photonic gap in periodic dielectric structures,” *Phys. Rev. Lett.*, vol. 65, no, 25, pp. 3152-3155, 1990.

17. W. M. Robertson, G. Arjavalingam, R. D. Meade, K. D. Brommer, A. M. Rappe, and J. D. Joannopoulos, “Measurement of photonic band structure in a two-dimensional periodic dielectric array,” *Phys. Rev. Lett.*, vol. 68, no. 13, pp. 2023-2026, 1992.

18. K. W. K. Shung and Y. C. Tsai, “Surface effects and band measurements in photonic crystals,” *Phys. Rev. B*, vol. 48, no. 15, pp. 1265-11269, 1993.

19. A. Mekis, J. C. Chen, I. Kurland, S. Fan, P. R. Villeneuve, and J. D. Joannopoulos , “High transmission through sharp bends in photonic crystal waveguides,” *Phys. Rev. Lett.*, vol. 77, no. 18, pp. 3787-3790, 1996.

20. M. Loncar, M. Hochberg, A. Scherer, and Q. Yueming, “High quality factors and room-temperature lasing in a modified single-defect photonic crystal cavity,” *Opt. Lett.*, vol. 29, no. 7, pp. 721-723, 2004.

21. H. Takano, Y. Akahane, T. Asano, and S. Noda, “In-plane-type channel drop filter in a two-dimensional photonic crystal slab,” *Appl. Phys. Lett.*, vol. 84, no. 13, pp. 2226-2228, 2004.

22. S. F. Mingaleev and Y. S. Kivshar, “Nonlinear transmission and light localization in photonic crystal waveguides,” *J. Opt. Soc. Am. B*, vol. 19, no. 9, pp. 2241-2249, 2002.

23. J. D. Joannopoulos, R. D. Meade, and J. N. Winn, *Photonic Crystals: Molding the Flow of Light*, Princeton, NJ: Princeton Univ. Press, 1995.

24. E. Yablonovitch, “Photonic crystals,” *J. Mod. Opt.*, vol. 41, no. 2, pp. 173-194, 1994.

25. S. John and M. Florescu, “Photonic bandgap materials: towards an all-optical micro-transistor,” *J. Opt. A: Pure Appl. Opt.*, vol. 3, no. 6, pp. S103-S120, 2001.

26. S. Fan and J. D. Joannopoulos, “Photonic crystals: towards large-scale integration of optical and optoelectronic circuits,” *Opt. and Phot. News*, vol. 11, no. 10, pp. 28-33, 2000.

27. J. Martorell, “Parametric nonlinear interaction in centrosymmetric three-dimensional photonic crystals,” *J. Opt. Soc. Am. B*, vol. 19, no. 9, pp. 2075-2082, 2002.

28. Y. Xu, R. K. Lee, and A. Yariv, "Propagation and second-harmonic generation of electromagnetic waves in a coupled-resonator optical waveguide," *J. Opt. Soc. Am. B*, vol. 17, no. 3, pp. 387-400, 2000.

29. Y. Dumeige, I. Sagnes, P. Monnier, P. Vidakovic, C. Mériadec, and A. Levenson, "$\chi^{(2)}$ semiconductor photonic crystals," *J. Opt. Soc. Am. B*, vol. 19, no. 9, pp. 2094-2101, 2002.

30. M. D. Rahn, A. M. Fox, M. S. Skolnick, and T. F. Krauss, "Propagation of ultrashort nonlinear pulses through two-dimensional AlGaAs high-contrast photonic crystal waveguides," *J. Opt. Soc. Am. B*, vol. 19, no. 4, pp. 716-721, 2002.

31. M. Soljačić, M. Ibanescu, S. G. Johnson, J. D. Joannopoulos, and Y. Fink, "Optical bistability in axially modulated OmniGuide fibers," *Opt. Lett.*, vol. 28, no. 7, pp. 516-518, 2003.

32. M. Soljačić, C. Luo, J. D. Joannopoulos, and S. Fan, "Nonlinear photonic crystal microdevices for optical integration," *Opt. Lett.*, vol. 28, no. 8, pp. 637-639, 2003.

33. M. Soljačić, S. G. Johnson, S. Fan, M. Ibanescu, E. Ippen, and J. D. Joannopoulos, "Photonic-crystal slow-light enhancement of nonlinear phase sensitivity," *J. Opt. Soc. Am. B*, vol. 19, no. 9, pp. 2052-2059, 2002.

34. G. Fibich, B. Ilan, and S. Tsynkov, "Backscattering and nonparaxiality arrest collapse of damped nonlinear waves," *SIAM J. Appl. Math.*, vol. 63, pp. 1718–1736, 2003.

35. K. S. Yee, "Numerical solution of initial boundary value problems involving Maxwell's equations in isotropic media," *IEEE Trans. Ant. and Prop.*, vol. 14, no. 3, pp. 302-307, 1966.

36. D. M. Sullivan, "Nonlinear FDTD formulations using *Z* transforms," *IEEE Trans. Micr. Theo. and Tech.*, vol. 43, no. 3, pp. 676-682, 1995.

37. P. Tran, "Optical switching with a nonlinear photonic crystal: a numerical study," *Opt. Lett.*, vol. 21, no. 15, pp. 1138-1140, 1996.

38. P. Tran, "Optical limiting and switching of short pulses by use of a nonlinear photonic bandgap structure with a defect," *J. Opt. Soc. Am. B*, vol. 14, no. 10, pp. 2589-2595, 1997.

39. M. Zitelli, E. Fazio, and Bertolotti, "All-optical NOR gate based on the interaction between cosine-shaped input beams of orthogonal polarization," *J. Opt. Soc. Am. B*, vol. 16, p. 214, 1999.

40. Y. H. Pramono, M. Geshiro, T. Kitamura, S. Sawa, "Optical logic OR-AND-NOT and NOR gates in waveguides consisting of nonlinear material," *IEICE Trans. Electron.*, vol. E83C, p. 1755, 2000.

41. Y. H. Pramono, Endarko, "Nonlinear waveguides for optical logic and computation," *J. Nonlinear Opt. Phys. Mater.*, vol. 10, p. 209, 2001

42. T. Yabu, M. Geshiro, T. Kitamura, K. Nishida, S. Sawa, "All-optical logic gates containing a two-mode nonlinear waveguide," *IEEE J. Quantum Electron.*, vol. 38, pp. 37-46, 2002.

43. T. Yabu, K. Nishida, M. Geshiro, S. Sawa, "All-optical logic elements containing nonlinear material," *Electron. Commun. Japan Part II-Electron.*, vol. 85, pp. 1, 2002.

44. S. Visnovsky, R. Lopusnik, M. Bauer, J. Bok, J. Fassbender, and B. Hillebrands, "Magnetooptic ellipsometry in multilayers at arbitrary magnetization," *Opt. Express*, vol. 9, no. 3, pp. 121-135, 2001.

45. A. Taflove and S. C. Hagness, *Computation Electrodynamics: The Finite-Difference Time-Domain Method*, Norwood, MA: Artech House, Inc., 2000.

46. M. Dinu, F. Quochi, and H. Garcia, "Third-order nonlinearities in silicon at telecom wavelengths," *Applied Physics Letters*, vol. 82, no. 18, pp. 2954-2956, 2003.

47. C. T. Chan, Q. L. Yu, K. M. Ho, "Order-N spectral method for electromagnetic waves," *Phys. Rev. B*, vol. 51, no. 23, pp. 16635-16642, 1995.

48. J. P. Berenger, "A perfectly matched layer for the absorption of electromagnetic waves," *J. Comput. Phys.*, vol. 114, no. 2, pp. 185-200, 1994.

49. A. C. Cangellaris, "Numerical stability and numerical dispersion of a compact 2-D/FDTD method used for the dispersion analysis of waveguides," *IEEE Micr. and Guid. Wv. Let.*, vol. 3, no. 1, pp. 3-5, 1993.

50. R. F. Remis, "On the stability of the finite-difference time-domain method," *J. Comput. Phys.*, vol. 163, no. 1, pp. 249-261, 2000.

51. Y. Amnon, P. Yeh, *Optical waves in crystals: propagation and control of laser radiation*, New York City, NY: Wiley, 1984.

52. V. Van and S. K. Chaudhuri, "A hybrid implicit–explicit FDTD scheme for nonlinear optical waveguide modeling," *IEEE Micr. and Theo. Tech.*, vol. 47, no. 5, pp. 540-545, 1999.

53. D. E. Merewether, R. Fisher, F.W. Smith, "On implementing a numeric Huygen's source scheme in a finite difference program to illuminate scattering bodies", *IEEE Trans. on Nuc. Sci.*, vol. 27, no. 6, pp. 1829-1833, 1980.

54. T. Baba and T. Iwai, "Enhancement of third order nonlinearity calculated for two-dimensional photonic crystal," *Jpn. J. Appl. Phys.*, vol. 42, no. 4A, pp. 1603-1608, 2003.

55. A. Yariv, Y. Xu, R. K. Lee, and A. Sherer, "Coupled-resonator optical waveguide: a proposal and analysis," *Opt. Lett.*, vol. 24, pp. 711-713, 1999.

56. R. D. Meade, A. Devenyi, J. D. Joannopoulos, O. L. Alerhand, D. A. Smith, and K. Kash, "Novel applications of photonic band gap materials: Low-loss bend and high Q cavities," *J. Appl. Phys.*, vol. 75, pp. 4753-4755, 1994.

57. A. Adibi, R. Lee, Y. Xu, A. Yariv, and A. Scherer, "Design of photonic crystal optical waveguides with single mode propagation in the photonic bandgap," *Electron. Lett.*, vol. 16, pp. 1376–1378, 2000.

58. A. Jafarpour, A. Adibi, Y. Xu, and R. K. Lee, "Mode dispersion in biperiodic photonic crystal waveguides," *Phys. Rev. B.*, vol. 68, pp. 233 102–233 105, 2003.